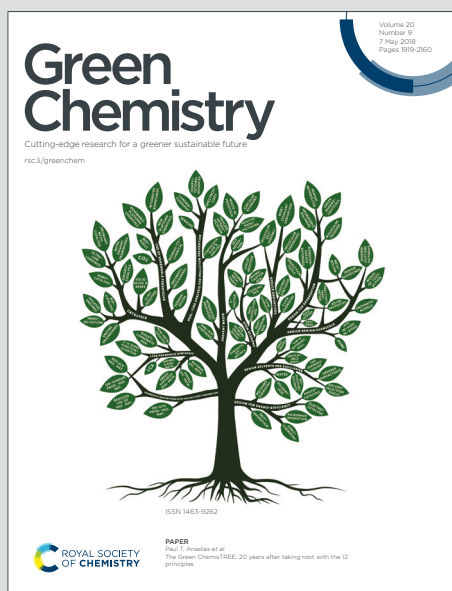


Green Chemistry

Cutting-edge research for a greener sustainable future

Accepted Manuscript

This article can be cited before page numbers have been issued, to do this please use: S. Zhou, F. Dai, C. Dang, M. Wang, F. Lu, D. Liu and H. Qi, *Green Chem.*, 2019, DOI: 10.1039/C9GC01720H.



This is an Accepted Manuscript, which has been through the Royal Society of Chemistry peer review process and has been accepted for publication.

Accepted Manuscripts are published online shortly after acceptance, before technical editing, formatting and proof reading. Using this free service, authors can make their results available to the community, in citable form, before we publish the edited article. We will replace this Accepted Manuscript with the edited and formatted Advance Article as soon as it is available.

You can find more information about Accepted Manuscripts in the [Information for Authors](#).

Please note that technical editing may introduce minor changes to the text and/or graphics, which may alter content. The journal's standard [Terms & Conditions](#) and the [Ethical guidelines](#) still apply. In no event shall the Royal Society of Chemistry be held responsible for any errors or omissions in this Accepted Manuscript or any consequences arising from the use of any information it contains.

Scale-up Biopolymer-Chelated Fabrication of Cobalt Nanoparticles Encapsulated in N-enriched Graphene Shells for Biofuel Upgrade with Formic Acid

Shenghui Zhou,^a Fanglin Dai,^{a,c} Chao Dang,^a Ming Wang,^a Detao Liu,^a Fachuang Lu,^a and Haisong Qi*,^{a,b}

^a State Key Laboratory of Pulp and Paper Engineering, South China University of Technology, Guangzhou 510640, China.

^b Guangdong Engineering Research Center for Green Fine Chemicals, Guangzhou 510640, China.

^c School of Chemistry and Chemical Engineering, Guangxi University, Nanning 530004, China.

Abstract: Both exploring high-performance catalytic materials from non-edible lignocellulosic biomass and selective hydrodeoxygenation of bioderived molecules will enable the value-added utilization of renewable feedstocks to replace rapidly diminishing fossil resources. Herein we developed a scale-up and sustainable method to fabricate gram-quantities of highly dispersed cobalt nanocatalysts sheathed in multilayered N-doped graphene (Co@NG) by using biomacromolecule carboxymethyl cellulose (CMC) as raw material. The ionic gelation of CMC, urea and Co²⁺ ions lead to the uniform dispersion and chelation of different species, consequently resulting in the formation of high distributed Co nanoparticles (NPs) (10.91 nm) with N-enriched graphene shells in solid-state thermolysis process. The usage of urea as non-corrosive activation agents can introduce a porous belt-like nanostructure and abundant doped nitrogen. Among all the prepared catalysts in this work, the optimized Co@NG-6 with the largest specific surface area (627 m² g⁻¹), the most and strongest basic sites, the highest proportion of pyridinic-N (37.6%) and mesopore exhibited excellent catalytic activity (99% yield of 2-methoxy-p-cresol) for base-free transfer hydrodeoxygenation (THD) of lignin molecule vanillin using bioderived formic acid (FA) as H source at 160 °C for 6 h. The poisoning tests and electron paramagnetic resonance spectra (EPR) verified that the strong interaction between N atoms and encapsulated Co NPs provided synergistic effects, which were essential for the outstanding catalytic performance of Co@NG-6. The deuterium kinetic isotope effect study clearly demonstrated the formation of Co-H⁻ via β-hydride elimination and protonation was rate-determining step, and the protic N-H⁺ and hydridic Co-H⁻ were considered to be active intermediate species in THD reaction. Furthermore, Co@NG-6 was highly stable for recycling owing to graphene shells preventing Co NPs from corrosion and aggregation.

1. Introduction

View Article Online
DOI: 10.1039/C9GC01720H

As global energy systems and traditional chemical industry gradually shift from depleted fossil fuels to renewable resources, an urgency exists to explore new technologies to drive the transformation of biomass to bio-fuels and industry-related green products.¹⁻⁴ The pyrolysis of lignocellulosic biomass is a prospective approach for producing valuable liquid bio-oil.⁵⁻⁸ As an effective strategy, hydrodeoxygenation is of vital importance for improving energy density of bio-oil by selectively removing oxygen-containing groups.⁹⁻¹²

The traditional hydrodeoxygenation technology requires explosive fossil resources-derived hydrogen gas that is dangerous and uncontrollable, often leading to overhydrogenation and C–C cleavage.¹³⁻¹⁶ In contrast, as a versatile renewable reagent with considerable H content (4.4 wt%), formic acid (FA) can be regarded as a secure, cheap and convenient liquid H source for THD.¹⁷⁻¹⁸ Notably, FA could be accessible from biorefinery processing, or by hydrogenation of CO₂.¹⁹⁻²¹ However, a large number of basic compounds (e.g., sodium/potassium salts, amines) were introduced as additives in most transition metal-catalyzed FA transfer hydrogenation processes. This can lead to the high expense in the separation and purification of target product.²²⁻²³ For instance, M. Beller and collaborator reported catalytic transfer hydrogenation of nitroaromatics with FA on cubane-type Mo₃S₄ cluster, but the base triethylamine was required.²⁴ Moreover, acidic FA can result in severe corrosion and leaching of catalytic active sites.²⁵ Therefore, it is significant to design an acid-resistant catalyst that is low-cost, sustainable and efficient for base-free THD of biomass molecules with FA.

In recent years, transition metal nanoparticles (e.g., Fe, Co, Ni and Ru) sheathed in graphene shells or carbon nanotubes have emerged as a novel catalyst (called as “chainmail catalyst”) and quickly attracted wide attentions due to their high activity and stability under harsh conditions.²⁶⁻²⁸ Bao and co-workers reported that the interaction between metallic core and graphene shells can change the work function of shell, and therefore endow it with superior chemical activities.²⁹ Later on, several materials have been reported for high-performance electrocatalysts for water splitting or evolution reactions.³⁰⁻³² However, most of preparation processes are uneconomical, such as the undesirable employment of expensive and non-renewable precursors, or the complicated preparation process (e.g. chemical vapor deposition) with high energy consumption or special instruments.³³⁻³⁴ These may limit its practical application.

Another important issue is the realization of large-scale production of catalysts to meet the needs of industrial applications, which remains a great challenge.³³⁻³⁴

Recently, several researchers have found that the edible monosaccharide or disaccharide (e.g. glucose, sucrose, fructose, D-xylose, D-glucosamine hydrochloride) can be used as building blocks for preparing analogous chainmail catalyst, indicating that fabrication of catalysts from natural resources has great advantages for practical applications owing to the low-cost, non-toxicity, renewability.³⁵⁻⁴⁰ Nevertheless, the use of monosaccharide as raw materials is a controversial issue since it is principally used as food or intermediate for drug synthesis.⁴¹ In contrary, the use of non-edible lignocellulosic biomass is more meaningful for the preparation of catalytic materials owing to the huge worldwide availability of plant-derived lignocelluloses including agricultural wastes and forest residues. The utilization and transformation of non-edible biomass components, such as lignin, cellulose and its derivatives, chitin, etc., into platform molecules and catalytic materials play a key role in sustainable development.⁴² However, compared with soluble glucose, most lignocellulosic biomass is insoluble in conventional solvents owing to the H bond interactions, making it difficult for the dispersion of active species and manufacture of catalysts.⁴³ Therefore, the application of non-edible lignocellulosic biomass as raw material for preparing chainmail catalyst is seldom reported. Cellulose, which is available from wood and agricultural residues, is abundant, low-cost, renewable and environmentally benign.⁴⁴ In our previous work, we tried cellulose as raw material and NaOH–urea aqueous solution as solvent to prepare a chainmail catalyst.⁴⁵ Although failed, we found this catalyst can effectively promote transfer hydrogenation of furfural. However, the agglomeration of large MnOx particles (100–200 nm) was unfavourable for the exposure of catalytic active sites. Besides, the massive use of corrosive strong bases NaOH as activating agent was not practical.

Carboxymethylcellulose (CMC) is a type of cellulose derived from carboxymethylation of the hydroxyl groups in cellulose molecules. It can dissolve in hot water and chelate with a variety of metal ions (e.g., Ca²⁺, Mg²⁺, Zr⁴⁺ and Fe³⁺) due to the existence of rich carboxyl groups.⁴⁶ Here, we developed a novel approach to synthesize gram-quantities of highly dispersed Co nanocatalysts sheathed by multilayered N-enriched graphene shells by pyrolysis of CMC. In this method, water-soluble CMC was chelated and gelled with urea and Co²⁺ ions, enabling the uniformly distribution and coordination of each component on the CMC chains. Consequently,

the solid-state thermolysis process of this precursors rendered the formation of highly dispersed Co NPs (10.91 nm) with N-enriched graphene shells (Co@NG). The urea acted as effective and non-corrosive activation agents, which introduced a porous structure with high specific surface area. More importantly, the doped-N derived from urea served as abundant basic sites to promote the reaction. Therefore, the prepared composite was a highly active and acid-tolerant catalyst for base-free THD of various biomass-derived organic compounds. The structural properties of as-prepared catalysts are systematically characterized by SEM, TEM, HAADF-STEM, XRD, BET, XPS, CO₂-TPD and Raman spectroscopy. To further investigate the THD mechanism by Co@NG-6, poisoning tests, EPR tests, deuterium kinetic isotope effect experiments were performed as well. In addition, heterogeneity tests of catalysts, leaching and recyclability experiments were also carried out.

2. Experimental Section

2.1 Materials and reagents

Sodium carboxymethyl cellulose (CMC) (M.W. 90000, 50-100 mPa.s), hydroxyethyl cellulose (250-450 mPa.s), hydroxypropyl cellulose (M.W. 100,000), methyl cellulose (40000 mPa.s), α -cellulose (25 μ m), Co(CH₃COO)₂·4H₂O (>99.0%), urea (>99.5%) were bought from Shanghai Macklin Biochemical Co., Ltd, China. Vanillin (>99.5%), furfural (>99.5%), vanillic alcohol (>99.0%), cinnamaldehyde (>99.5%), phenylpropyl aldehyde (>99%), benzaldehyde (>99%), phenylacetaldehyde (>99%), quinoline (>99.0%), nitrobenzene (>99.0%) were obtained from Aladdin Industrial Corporation. 95 wt.% DCOOD in 5 wt.% D₂O (98 atom % D), 95 wt.% DCOOH in 5 wt.% D₂O and 95 wt.% HCOOD in 5 wt.% D₂O were bought from the Sigma-Aldrich Industrial Corporation.

2.2 Synthesis of different samples

Preparation of catalysts. The N-enriched graphene shells encapsulated cobalt nanocatalysts (Co@NG) were fabricated according to the following method. Typically, 0.93 g CMC were dissolved in 60 mL distilled hot water (100 °C) under mechanical agitation to get a sticky and transparent CMC solution. Afterwards, 0.15g Co(CH₃COO)₂·4H₂O and 6.5 g urea were completely dissolved in ultrapure water. This purple solution was added to the previous CMC solution under mechanical agitation for 4 min. This CMC gel was then heated for ionic gelation and further dehydration at 70 °C in an oven for 20 h. Subsequently, the obtained dry block was smashed, placed in a

covered porcelain boat, followed by pyrolysis in a horizontal tube furnace at 800 °C for 2 h at a heating rate of 10 °C·min⁻¹ under N₂ flow. The carbonized samples were magnetic stirred in 60 mL hydrochloric acid solution (7 wt.%) for 12 h to remove residual chemicals and soluble cobalt. Then, the sample was separated by filtration and totally washed with ultrapure water until the filtrate was neutral. After drying in vacuum at 60 °C for 10 h, the sample was marked as Co@NG-6. For other Co@NG-U, U stands for the amount of added urea when 1g CMC was used as carbon source. Replacing Co(CH₃COO)₂·4H₂O with other metal salts (Mn(CH₃COO)₂·4H₂O, Ni(CH₃COO)₂·4H₂O or Fe(NO₃)₃·9H₂O) synthesized Mn@NG, Ni@NG or Fe@NG, respectively. Replacing CMC with hydroxypropyl cellulose (HPC), microcrystalline cellulose (MCC), methyl cellulose (MC) or hydroxyethyl cellulose (HEC) synthesized Co@NG-HPC, Co@NG-MCC, Co@NG-MC or Co@NG-HEC. The preparation procedure of nitrogen-doped carbon (NC-6) was same as that of Co@NG-6, but no Co(CH₃COO)₂·4H₂O was added in CMC solution.

A scale-up fabrication of Co@NG-6. The process route was same as that of Co@NG, except for increasing the added amount of CMC, Co(CH₃COO)₂·4H₂O, urea and distilled water to 5 g, 0.8g, 35g and 300 mL, respectively. The obtained dry block as precursors were carbonized in tube furnace in twice. It is worth noting that the formed and sublimated carbon nitride during preparation may block the gas outlet. Hence, the tube diameter of the outlet is 1 cm. Finally, 1.74 g Co@NG-6 catalysts can be obtained (**Figure S1**). Due to the facile preparing process and the use of low-cost and abundant biomass as raw material, this synthesis method can be expected to realize the large-scale production for industrial application.

2.3 Catalyst characterization

The texture structures of as-prepared catalysts were evaluated by low temperature N₂ adsorption–desorption at -196 °C using a Micromeritics ASAP 2020. Before measurements, the catalysts were outgassed at 120 °C for 7 h. The BET specific surface areas were calculated using the Brunauer–Emmett–Teller method. The average pore volume and pore size were obtained by multipoint Barrett–Joyner–Halenda (BJH) method. X-ray diffraction (XRD) patterns were carried out using a Rigaku diffractometer (D/MAX/III A, 3 kW) with Cu K α radiation ($\lambda = 0.1543$ nm, 40 kV, 30 mA). The cobalt content of the catalysts was measured with Spectro Arcos FHX22 inductively coupled plasma-optical emission spectrometer (ICP-OES). The structures

and morphologies of samples were characterized by a high-resolution scanning electron microscopy (SEM, MERLIN of ZEISS) and a high-resolution transmission electron microscope (JEM-2100F) with EDX analysis (Bruker Xflash 5030T) operated at 200 kV. Raman spectra were obtained on a confocal laser LabRAM Aramis Raman Spectrometer (HORIBA Jobin Yvon) operating with 532 nm excitation and the wave number range used in the measurement was from 400 to 2000 cm^{-1} . X-ray photoelectron spectroscopy (XPS) were carried out on a Kratos Axis Ultra DLD system with a base pressure of 10^{-9} Torr. The surface basicity of catalysts was measured via temperature-programmed desorption of CO_2 (CO_2 -TPD) via a Micromeritics AutoChem II 2920 instrument. The catalyst was pretreated under a flow of helium gas ($30 \text{ mL} \cdot \text{min}^{-1}$) at 140°C for 2 h. Subsequently, the catalyst was cooled to 50°C under helium gas. After adsorption of carbon dioxide, the catalyst was flushed off under a He atmosphere at 50°C . Finally, the TPD data were obtained from 50°C - 750°C under helium gas (heating rate of $20^\circ\text{C} \cdot \text{min}^{-1}$). Electron paramagnetic resonance (EPR) spectra were performed on a Bruker EMX spectrometer. The EPR experiments were conducted with a center field of 3507.815 G and a frequency of 9.83 GHz using an Elexsys probe head with 20 mg of catalyst in a 4 mm tube. The water contact angle of samples was analyzed using a drop shape analysis system (Krüss, DSA100).

2.4 Procedures for THD of vanillin

The THD process of vanillin was performed in a glass tube reactor (25 mL) under oil-heating conditions. Typically, vanillin (0.5 mmol), water (10 mL), and catalyst (50 mg) were added into the glass tube reactor. This reactor was then purged with nitrogen gas and sealed. Afterward, the reactor was placed in a preheated oil bath pot. After the THD reaction for a desired time under magnetically stirring, the reactor was rapidly transferred into cold water. The liquid aqueous mixtures were collected and extracted by ethyl acetate for analysis. We used GC-MS (Agilent 7890B-5977A) equipped with HP-5MS capillary column ($30.0 \text{ m} \times 250 \text{ mm} \times 0.25 \text{ mm}$) to identify the products in the reaction mixture. We used GC (Shimadzu Nexis GC-2030) equipped with flame ionization detector and HP-5 capillary column ($30.0 \text{ m} \times 250 \text{ mm} \times 0.25 \text{ mm}$) to quantitatively analyze the reactants and products on the basis of standard samples.

2.5 Catalyst recycling experiments

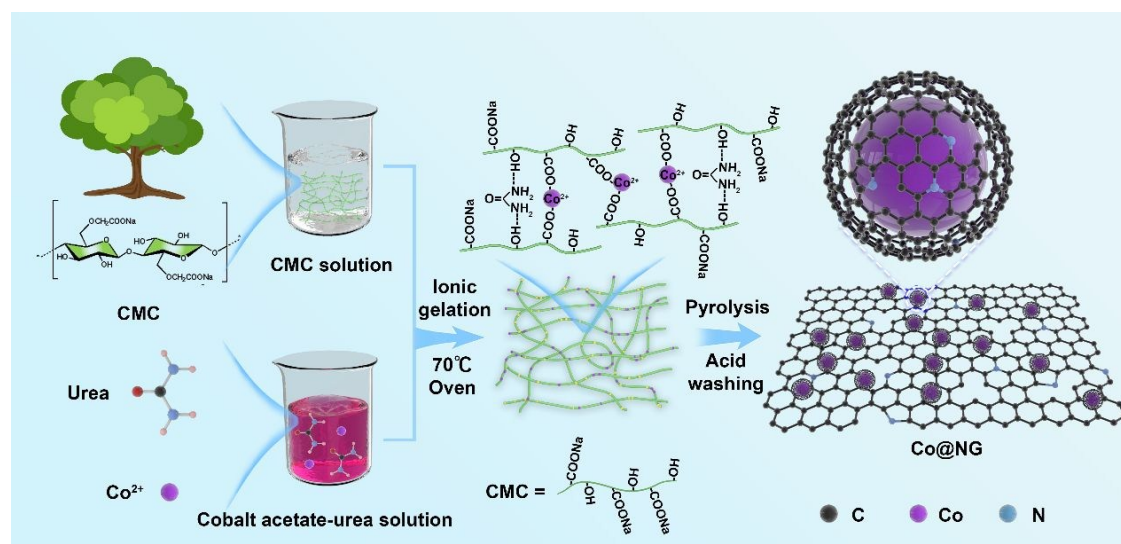
After THD reaction, the catalysts were isolated from reaction products by a magnet, washed several times with distilled water, ethyl acetate, and ethanol and dried in a vacuum drying oven at 50 °C. Furthermore, the recycled catalysts were kept for the next cycle directly under the identical reaction conditions without further treatment.

2.6 Deuterium kinetic isotope effect experiments

For deuterium kinetic isotope effect experiments of THD of vanillin, we used different deuterated formic acid (HCOOH, HCOOD, DCOOH and DCOOD) as H source to demonstrate the transfer hydrodeoxygenation mechanism and the rate-limiting step. After the THD reaction, the reaction products were extracted by ethyl acetate and analyzed by GC (Shimadzu Nexis GC-2030) and GC-MS (Agilent 7890B-5977A).

3. Results and Discussion

3.1 Characterization of catalysts



Scheme 1. The fabrication process of Co@NG.

The schematic illustration for the in-situ preparation of Co@NG catalysts is depicted in **Scheme 1**. The utilization of CMC is particularly meaningful not only for its renewable feature but also the intrinsic abundant carboxyl and hydroxyl groups for further gelation by chelating with Co²⁺ ions and urea. After the gelling processes, CMC chains can be aggregated into interconnected nanofibrils with uniform coordination of Co²⁺ and urea. During the thermolysis process of dry precursors, CMC transformed into carbons and urea decomposed and released NH₃ and CO₂. The resulting gases can activate the carbon skeleton and trigger nitrogen doping. Co²⁺ ions can be reduced by carbon into high dispersed Co NPs, which can serve as catalysts promoting the

formation of N-enriched graphene shells. Gram-scale quantity of Co@NG can be obtained by one run, indicating the feasibility for realizing bulk production of this catalyst (**Figure S1**).

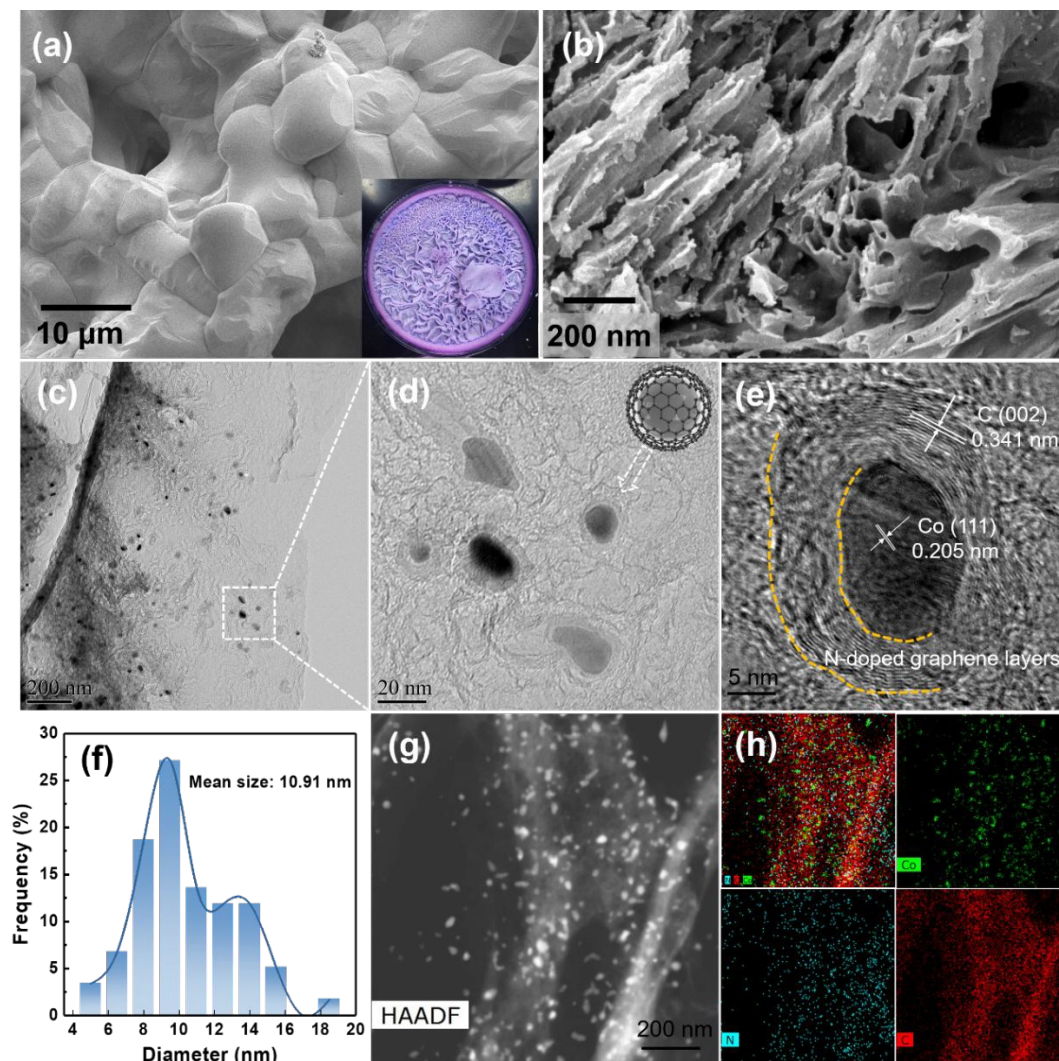


Figure 1. SEM images of unpyrolyzed Co@NG-6 precursor (a) (the insert is digital photo). SEM image of Co@NG-6 (b). Typical TEM image (c, d), high-resolution TEM image (e), particle-size distribution histogram (f), HAADF-STEM image (g), and elemental mapping (g) of Co@NG-6.

Afterwards, the physical–chemical properties of Co@NG-U (U stands for the amount of added urea) were characterized by several techniques to clarify the relationship between the structure of as-prepared catalysts and their catalytic reactivity. The morphologies and metal dispersions of the samples were analyzed by scanning electron microscopy (SEM) and transmission electron microscopy (TEM). As can be seen from **Figure 1a**, the flower-like unpyrolyzed Co@NG-6 precursor confirmed tightly bind of three components (CMC, urea and Co^{2+} ions) after ionic gelation and chelation process.

Without urea, or CMC, the precursor is a flat sheet or scattered rod shape (**Figure S2a, b**). Moreover, NC-6 precursor also showed the shape of interlinked polymers, indicating the chelation of CMC and urea (**Figure S2c**). After the pyrolysis process, Co@NG-0 without urea exhibited an overall block structure with very few interconnected macropores (**Figure S3a**). In contrary, Co@NG-6 and NC-6 all showed typical three-dimensional hierarchical porous nanostructure with abundant continuously cross-linked mesopores and macropores (**Figure 1b, S3b**). Other samples (Mn@NG-6, Fe@NG-6, Ni@NG-6) all showed similar morphologies with a large number of channels (**Figure S3c-e**). This result indicated that the gelation and chelation of CMC, urea and Co^{2+} ions and presence of urea in preparing catalysts can promote the formation of uniform porous structure by releasing NH_3 and CO_2 , thus activating the carbon skeleton.

TEM images in **Figure 1c, f** showed that the metallic Co NPs with a mean diameter of 10.91 nm were well-distributed in carbon skeleton. Further high-resolution (HRTEM) analysis indicated that Co NPs were well encapsulated inside 3-10 layers of graphene shells with obvious interlayer distance of 0.341 nm. All Co NPs had a diameter of ~ 7 nm and displayed a clear lattice fringe with interplanar distance of 0.205 nm, which could be assigned to (111) plane of β -Co (**Figure 1d, e**). Obviously, in this encapsulated catalyst, the electron of Co core could penetrate through the self-catalysis-formed graphene surface to boost the catalytic process on external graphene shell. Meanwhile, the graphene layers acted as shells can prevent reaction substrates from contacting the Co core and therefore can protect the Co core from corrosion and aggregation during the following harsh acidic THD reaction conditions.⁴⁷ The HRTEM-EDS (energy-dispersive X-ray spectrometry) in **Figure S4** confirmed sample was consisted of four components, that is Co, N, C, and O. The EDS elemental mapping from representative high-angle annular dark-field scanning TEM (HAADF-STEM) validated uniform distribution of Co, N and C in Co@NG-6 (**Figure 1g, h**).

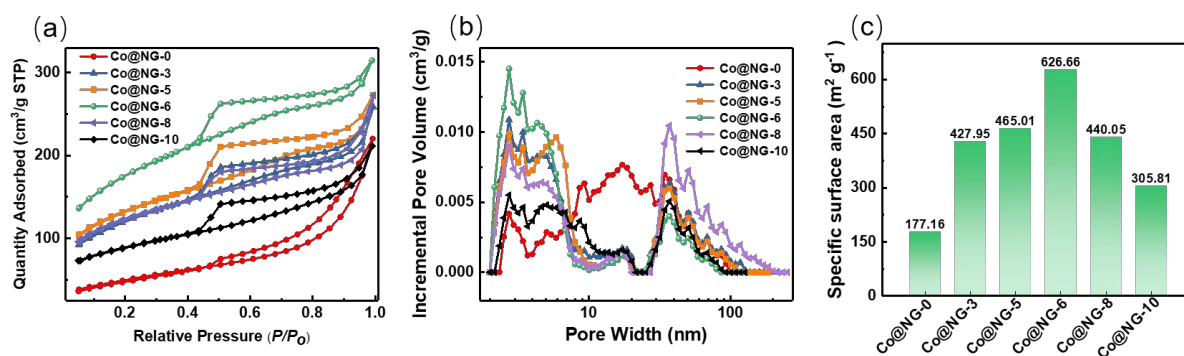


Figure 2. N₂ adsorption-desorption isotherms (a), corresponding pore size distributions (b) and specific surface area (c) of Co@NG-U.

The porous properties of Co@NG-U were examined by nitrogen adsorption/desorption analysis. The isotherm curves can be assigned to typical type IV patterns with a characteristic hysteresis loop at high relative pressures, demonstrating the existence of abundant mesopores in all Co@NG-U samples (**Figure 2a**). The BJH pore size distribution calculated from the adsorption branch of the isotherms (**Figure 2b**) showed that all the samples exhibited intensive pore size distribution centered at ~2–100 nm, confirming the hierarchical porous structure. Notably, as the elevated amount urea from 0 g to 6.5 g, the specific surface area increased remarkably from 177.16 to 626.66 m² g⁻¹ and the pore size changed from macropore to mesopore (**Figure 2c**). However, the continuous increase of urea led to the obvious decline of specific surface area and pore volume. This is because CMC transformed into amorphous carbons and urea decomposed and released NH₃ and CO₂ in the pyrolysis process. The resulting gases can etch the carbon skeleton, thus promoting the formation of porous structure and high specific surface area, simultaneously triggering nitrogen doping. Further increasing the amount of urea to a high level, however, the structure of carbon skeleton was broken and collapsed, resulting in the decrease of specific surface area.

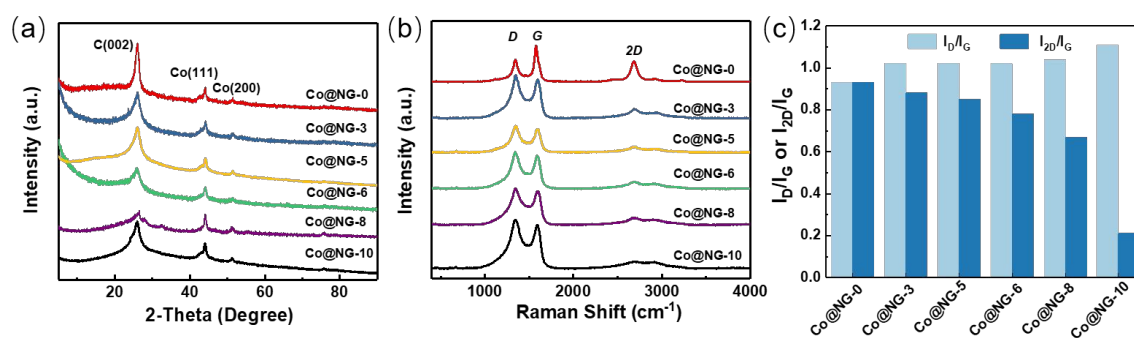


Figure 3. XRD patterns (a), Raman spectra (b), I_D/I_G and I_{2D}/I_G ratios (c) of Co@NG-U.

The XRD patterns in **Figure 3a** showed an obvious diffraction peak at 26.1°, which was assigned to (002) reflection of crystallized carbon. Besides, the characteristic diffraction peaks at 44.3° and 51.4° could be ascribed to (111) and (220) reflections of detectable cubic cobalt, respectively. Raman spectroscopy was performed to get more insights into the graphitic degree and defects of Co@NG. Three pronounced peaks at 1350, 1580 and 2750 cm⁻¹ in **Figure 3b** could be ascribed to D, G and 2D bands of carbon materials, respectively. From the comparison of I_D/I_G ratios and I_{2D}/I_G , it can be

seen that the I_D/I_G ratios value increased and I_{2D}/I_G decreased when the amount of added urea increased from 0 g to 10 g, indicating the increase of defective structure in carbon materials (**Figure 3c**).

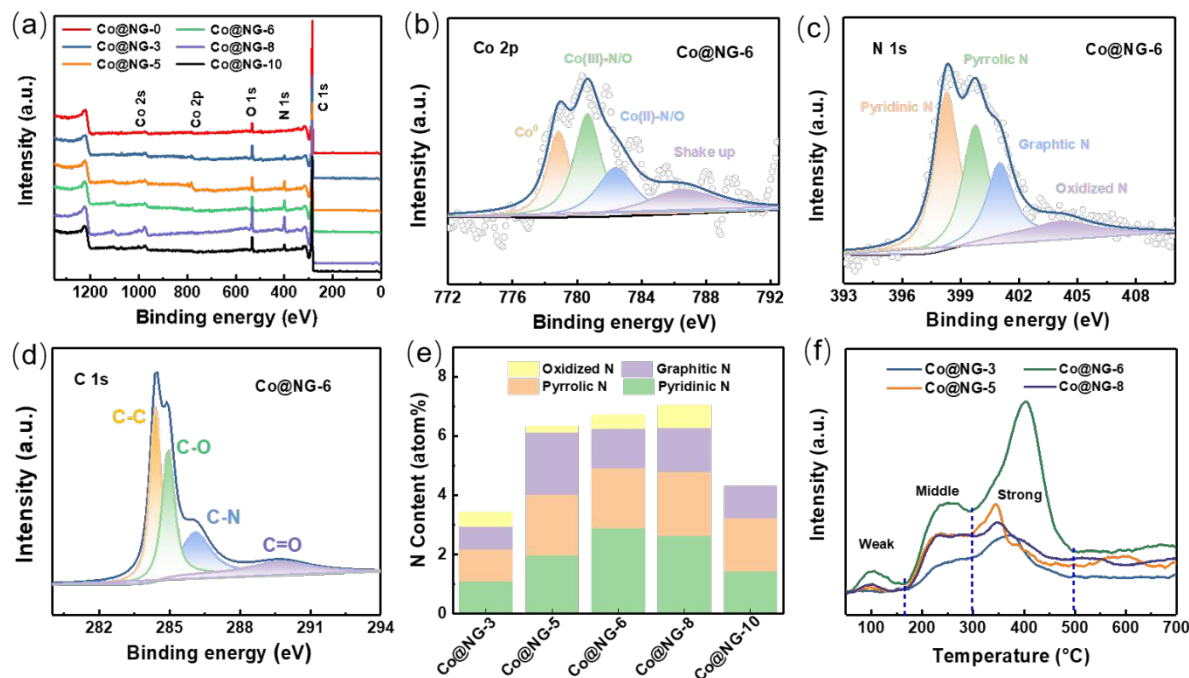


Figure 4. XPS spectrum of survey scan of Co@NG-U samples (a); High-resolution Co 2p (b), N 1s spectrum (c), C 1s spectrum (d) of Co@NG-6; Configurations of N dopants (e) and CO₂-TPD (f) of Co@NG-U.

X-ray photoelectron spectroscopy (XPS) investigations indicated that Co@NG-U consisted of Co, N, C and O (**Figure 4a**). As manifested in **Figure 4b** and **S5**, the Co 2p spectrum of Co@NG could corroborated the coexistence of three cobalt species, metallic Co (778.6 eV), Co(III)-N/O (780.5 eV) and Co(II)-N/O (782.5 eV). The existence of Co-O/Co-N confirmed the strong interaction between Co species and N-doped graphene shell via Co-O-C or Co-N-C bonds, which resulting in lower electron density in cobalt site. The percentage of Co⁰ increased from 17.3% to 35.0% with an increased amount of urea from 0 g to 6.5 g but then decreased to 27.6% at 10 g. This indicated that the generated NH₃ from urea can reduce Co ions into Co⁰. The Co⁰ species are the active sites in transfer hydrogenation reaction.^{18, 25} However, the excess NH₃ can also promote the formation of Co(III)-N species. Furthermore, the N 1s spectrum of Co@NG suggested that there existed four N species, pyridinic N (398.6 eV), pyrrolic N (400.6 eV), graphitic N (401.2 eV) and pyridine oxide N (403.9 eV) (**Figure 4c**, **S6**). Co@NG-6 possessed highest content of pyridinic N sites and

Co@NG-8 had the maximum nitrogen content (**Figure 4e**, **Table S2**). The C 1s spectrum of Co@NG could be deconvoluted into three peaks located at 284.4, 285.6, and 288.6 eV, which could be indexed to C-C, C-N and C-O bonds, respectively (**Figure 4d**). The presence of C-N bond verified the successful introduction of nitrogen in carbon skeleton. In addition, we further carried out CO₂-TPD to measure the surface basicity of catalysts. As can be seen in **Figure 4f**, Co@NG-6 exhibited the highest strength and density of basic site in all samples based on the temperature and peak area of carbon dioxide-desorption peaks. All these Co@NG-U samples had a similar Co content of around 1 wt% on the basis of inductively coupled plasma optical emission spectrometry (ICP-OES) results in **Table S1**. The nitrogen content of Co@NG-U catalysts was determined to be between 0.2 and 7.04 at% from Co@NG-0 to Co@NC-8, respectively, based on XPS results (**Table S1**). Further elevating the amount of urea in preparing the catalyst did not lead to a higher nitrogen content of Co@NG, but resulted in a lower yield of Co@NG catalysts due to the over etching of carbon skeleton by generated gases from urea.

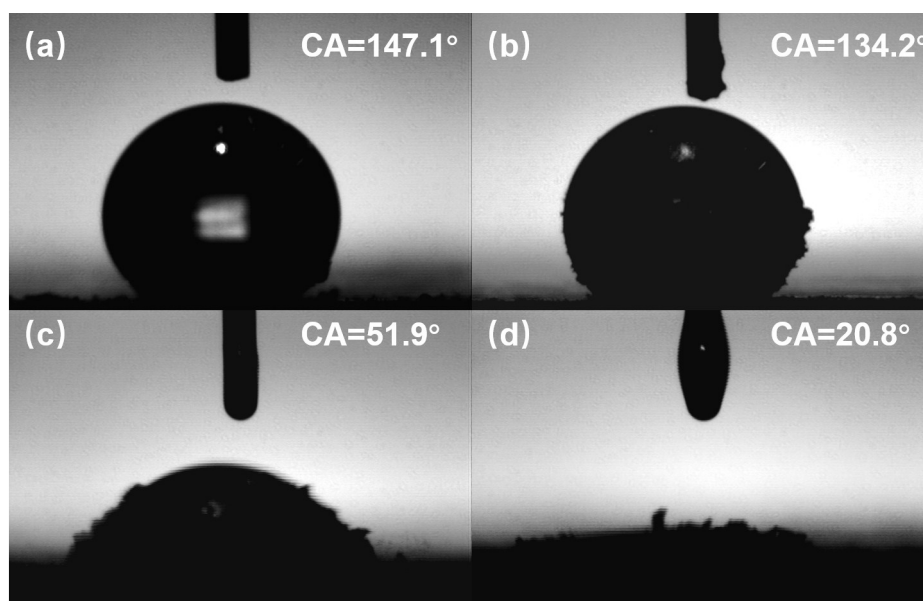


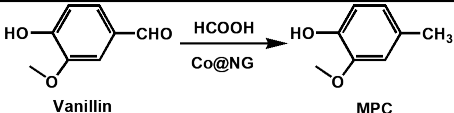
Figure 5. Photographs of a water droplet with a contact angle of Co@NG-0 (a), Co@NG-3 (b), Co@NG-6 (c), Co@NG-8 (d).

The wettability of prepared Co@NG catalysts was studied using water contact angle measurement method and the results were present in **Figure 5**. Co@NG-0 and Co@NG-3 without N-doping or low N-doping displayed hydrophobicity with a high contact angle of about 147.1° and 134.2°, respectively. In contrary, Co@NG-6 and Co@NG-8 all displayed superhydrophilicity with low contact angle of 51.9° and 20.8°.

In addition, a digital photo in **Figure S7** showed that Co@NG-6 can be well-dispersed in water due to the doped N increased the hydrophilic property, which might enhance the exposure of catalyst to vanillin, thereby significantly increasing the catalytic performance.

3.2 Evaluation of the catalytic performance of the various catalysts

Table 1. Catalytic results for different catalysts.^a

Entry	Catalysts				MPC		
		Conversion	MPC selectivity	MPC yield	formation rate	TOF	FA eff.
		(%)	(%)	(%)	(mmol g ⁻¹ h ⁻¹) ^b	(h ⁻¹) ^c	(%) ^d
1	Blank	0	0	0	0.0	-	0
2	Co Powder	3.2	93	3.0	59.5	0.28	0.5
3	Co(OAc) ₂	2.1	92	1.9	38.6	0.18	0.4
4	C Powder	0	0	0.0	0.0	-	0.0
5	NC-6	9.3	100	9.3	186.0	-	1.7
6	Co@NG-0	0.4	99	0.4	7.9	0.03	0.1
7	Co@NG-3	23.3	100	23.3	466.0	2.03	4.3
8	Co@NG-5	25.1	100	25.1	502.0	2.18	4.6
9	Co@NG-6	57.1	100	57.1	1142.0	4.97	10.5
10 ^e	Co@NG-6	98.5	100	98.5	820.8	3.57	18.1
11	Co@NG-8	55.3	100	55.3	1106.0	4.81	10.2
12	Co@NG-10	39.4	100	39.4	788.0	3.43	7.3
13	Mn@NG-6	3.4	99	3.4	67.3	0.30	0.6
14	Fe@NG-6	13.6	100	13.6	272.0	1.18	2.5
15	Ni@NG-6	1.5	100	1.5	30.0	0.13	0.3
16	Co@NG-HEC	49.0	100	49.0	980.0	4.26	9.0
17	Co@NG-HPC	48.2	100	48.2	964.0	4.19	8.9
18	Co@NG-MC	36.7	100	36.7	734.0	3.19	6.8
19	Co@NG-MCC	11.5	99	11.4	227.7	1.00	2.1

^a Reaction conditions: 0.5mmol vanillin in 10 mL water, 250 mg FA, catalyst (2.3 mol% metal), 160 °C, 5 h. ^b MPC formation rate is defined as (mol of formed MPC)/(catalyst amount × time). ^c TOF is defined as mol (converted vanillin)/[mol (total

metal added) \times h (time)].^d The efficiencies of FA (FA eff.) were calculated taking into account that 1 mol of FA is needed to produced 0.5 mol of MPC.^e 6 h, catalyst (4.6 mol%).

Subsequently, vanillin, a representative model compound of liquid bio-oil from biomass lignin was used as a substrate to investigate the THD performance of various catalysts with FA as H source. The blank experiment revealed that the THD reaction did not take place without catalyst (**Table 1, Entry 1**). Then, different cobalt-containing compounds (Co Powder and Co(OAc)₂) were tested. All these Co catalysts failed to catalyze this THD reaction (**Table 1, Entries 2-3**). Compared to the carbon powder catalyst without nitrogen doping, NC-6 acquired a slight conversion of vanillin (9.3%), suggesting that nitrogen species were favorable for promoting the transfer reduction of vanillin (**Table 1, Entries 4-5**). The importance of nitrogen species in improving the activity will be discussed in the part of **Mechanism study**. Gratifyingly, the as-fabricated Co@NC-6 gave the highest conversion (57.1%) with 100% selectivity to 2-methoxy-*p*-cresol (MPC) with the highest formation rate (1142 mmol g⁻¹ h⁻¹) and TOF (4.97 h⁻¹) at 160 °C for 5 h among all tested samples (**Table 1, Entry 9**). Moreover, when the metal center Co of Co@NG-6 was replaced with other metals such as Mn, Fe and Ni, the conversion rate for THD of vanillin with FA decreased distinctly (**Table 1, Entries 13-15**). It not only confirmed that Co NPs were catalytic active center in THD, but also revealed that the nature of metallic catalytic center was critical for this reaction. After optimizing the reaction conditions, the THD of vanillin can obtain a near quantitative yield (98.5%) with the highest FA efficiency (18.1%) (**Table 1, Entry 10**). Moreover, the conversion of vanillin was remarkably increased from 0.4% to 57.1% as the amount of urea added in preparation process being increased from 0 to 6.5 g. However, further increasing the initial loading amounts of urea gradually decreased the vanillin conversion (**Table 1, Entries 6-12**). There were two main reasons accounting for the best performance of Co@NG-6 combined with the previous characterization: (1) The calculated BET surface area of Co@NG-6 was the highest (626.66 m² g⁻¹) along with the maximum pore volume and highest mesoporous proportion, which would be favorable for exposing more catalytic active sites and improving the adsorption and transformations of reaction substrate. (2) Co@NG-6 had the most and strongest basic sites (CO₂-TPD from **Figure 4f**) along with the highest proportion of pyridinic N (XPS from **Figure 4e**). The doped-nitrogen (especially electron-rich pyridinic N) can promote the electrons transfer from N-doped carbon/graphene to

transition metal, reduce the energy barrier for reactant adsorption, thus boosting the catalytic reaction.⁴⁸⁻⁴⁹ (3) It is noteworthy that Co@NG-8 also exhibited excellent catalytic performance although a little worse than Co@NG-6. The possible reasons are that Co@NG-6 also possess high content of N and defective structure along with high superhydrophilicity. This result revealed that urea loading played a crucial role on modulating the physical microstructure and chemical properties of final pyrolytic product, thus remarkably influencing the THD reaction.

3.3 Effect of different cellulose derivatives on catalysts

In order to reveal the importance of dissolution, chelation and gelation process of CMC, other cellulose derivatives including insoluble microcrystalline cellulose (MCC), soluble hydroxypropyl cellulose (HPC), hydroxyethyl cellulose (HEC) and methyl cellulose (MC) were respectively used as carbon source (**Table 1, Entries 16-19**). The as-prepared Co@NG-MCC gave a slightly improved vanillin conversion, indicating the complete dissolution of biomass macromolecule was important for the highly dispersion of each components. Co@NC-HEC and Co@NC-HPC with hydroxyethyl and hydroxypropyl groups in HEC and HPC exhibited comparable vanillin conversion (48~49%), formation rate (960~980 mmol g⁻¹ h⁻¹) and TOF (4.1~4.3 h⁻¹), while Co@NC-MC only gave moderate activity (36.7% conversion) compared to Co@NG-6. These results indicated that the dissolution, dispersion, chelation (carboxy, or hydroxyl with urea and Co²⁺) and gelation process of biomass precursors played an important role in homogeneous coordination and dispersion of active sites.

3.4 Effect of solvents and reaction conditions

Owing to that the solvents play an important role in determining reaction rate and product selectivity, we tried various solvents in THD of vanillin. The corresponding conversion, selectivity and polarity of solvents are depicted in **Figure 6a**. We found that strongly polar water and N, N-dimethylformamide (DMF) as solvent provides better conversion than low polar solvents, such as tetrahydrofuran (THF), 1,4-dioxane, and ethyl acetate. This law was consistent with the reported study that high polar solvents benefit from the hydrogenation of less polar substrates.³⁵ On the other hand, a digital photo in **Figure S7** showed that Co@NG-6 can be well-dispersed in water due to the doped N increased the hydrophilic property (confirmed by Contact angle measurement in **Figure 5**). The good dispersion capability in solvent water might

enhance the exposure of catalyst to vanillin, thereby significantly increasing the catalytic performance. Besides, water is an ideal green solvent that is environmentally friendly and low-cost when compared with DMF.

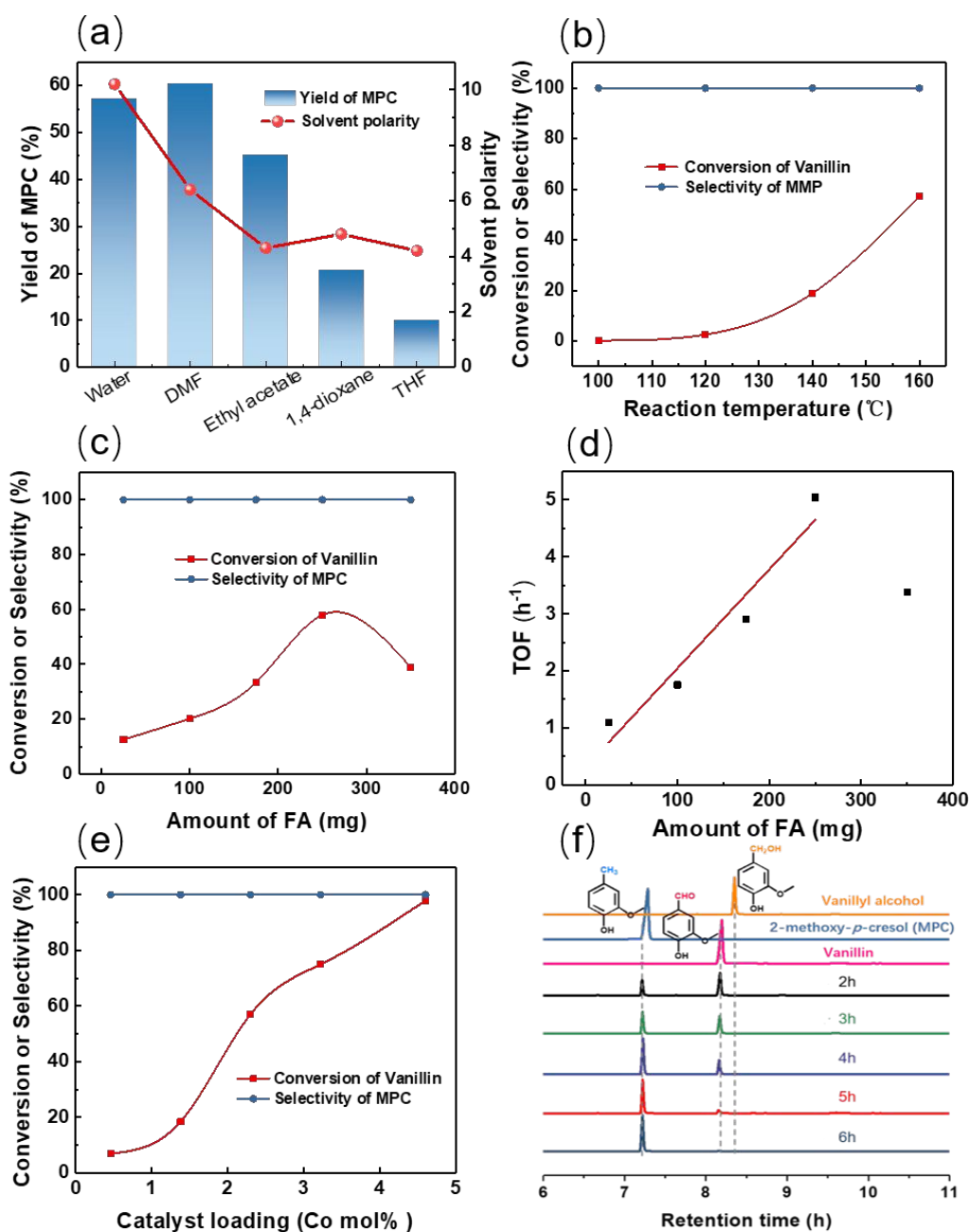


Figure 6. Optimization of THD reaction parameters. Reaction conditions: (a) 0.5 mmol vanillin in 10 mL solvent, 250 mg FA, Co@NG-6 catalyst (2.3 mol% metal), 160 °C, 5 h; (b) 0.5 mmol vanillin in 10 mL water, 250 mg FA, Co@NG-6 catalyst (2.3 mol% metal), 5h; (c) 0.5mmol vanillin in 10 mL water, Co@NG-6 catalyst (2.3 mol% metal), 160 °C, 5 h; (d) TOF values for conversion of vanillin with amount of FA. (e) 0.5mmol vanillin in 10 mL water, Co@NG-6, 250 mg FA, 160 °C, 5 h. (f) GC spectrum of the

conversion of vanillin with varied reaction time. 0.5mmol vanillin in 10 mL water, 250 mg FA, 160 °C, Co@NG-6 catalyst (4.6 mol% metal).

The reaction temperature significantly affected THD of vanillin (**Figure 6b**). The conversion over Co@NG-6 increased sharply from 0 to 57.1% when elevating the reaction temperature from 100 to 160 °C. Due to the use of glass reactor, the reaction temperature was not raised further. As the FA amount increased from 0 to 250 mg (**Figure 6c**), the vanillin conversion increases remarkably. Further increasing the FA amount to 350 mg, however, resulted in an obvious decrease of conversion to 37%, indicating the high concentration of FA can aggravate the etching, leaching and inactivation of Co NPs. The plot of reaction rate (TOF value) versus the concentration of FA is depicted in **Figure 6d**. The THD reaction rate followed a linear relationship versus the concentration of FA over the range 25–250 mg. The first-order dependence of the H source suggested a reaction mechanism in which the proton and/or hydride transfer is involved in, or precede, the rate-determining step. Further insights about the transfer hydrodeoxygenation mechanism over Co@NG-6 will be discussed in the part of **Reaction mechanism studies**.

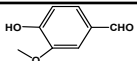
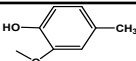
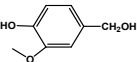
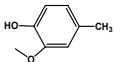
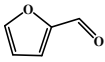
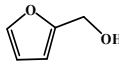
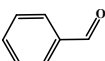
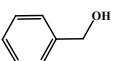
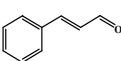
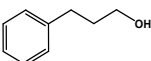
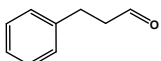
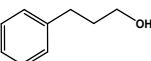
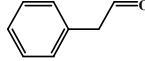
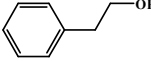
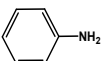
Catalyst loading and reaction time both has a large impact on the catalytic activity (**Figure 6e and S8**), and an increasing catalyst usage or reaction time led to the complete conversion of vanillin. Moreover, it is worth mentioning that no vanillyl alcohol was formed and MPC selectivity remains >99.0% in all reaction (**Figure 6f**). This result suggested a different reduction mechanism in comparison to other report using H₂ as H source, in which vanillyl alcohol is firstly generated and then hydrogenated to MPC.⁵⁰ The possible reasons will be discussed in the part of **Reaction mechanism**. Compared with the recent other reported noble metal-based catalysts using high pressure H₂ as H source (**Table S4**), our developed catalytic system with liquid H donor FA can also produce nearly quantitative MPC yield (99%) under mild conditions. Compared with the recent reported Co-based catalyst or the THD reaction using alcohols as H donors, the Co@NG-6 can also provide high conversion at lower reaction temperatures with less amount of catalyst (4.6 mol% Co).

3.6 Extension of the catalyst system.

The catalytic transfer hydrogenation of a series of unsaturated compounds was investigated further. For vanillyl alcohol, the reaction rate is faster than that of vanillin and only 2.5 h was needed to complete the transformation (**Table 2, Entries 2**).

Furthermore, Co@NG-6 was also broadly applicable for transfer reduction of other lignocellulose-derived oxygenates. For instance, the conversions of furfural, benzaldehyde were 100% and selectivities to the target alcohols were more than 90% (Table 2, Entries 3-4). Additionally, the developed Co@NG-6 also exhibited also superior catalytic performance for cinnamaldehyde resulting in more than 98% conversion with 96% selectivity to cinnamyl alcohol (Table 2, Entries 5). These reduced alcohols are significant reagents for preparing pharmaceuticals, flavors and cosmetics in fine chemical industry.⁵¹⁻⁵² Besides the THD of bioderived platform molecules, other unsaturated chemical compounds from petrochemical industry were also tested as substrates to evaluate the catalytic reactivity of Co@NG-6 (Table 2, Entries 6-9). For quinoline, the catalyst also exhibited outstanding catalytic activity and the yield of 1,2,3,4-tetrahydroquinoline are more than 96%. Because of the high value of aniline,⁵³ catalytic transfer hydrogenation of nitrobenzene was carried out and 90.8% yield of aniline was achieved within 6 h. Therefore, we concluded that Co@NG-6 was a highly versatile catalyst for catalytic THD of both bioderived chemicals and organic compounds from petrochemical industry with FA as H donor.

Table 2. Results of Co@NG-6-catalyzed transfer hydrogenation of various unsaturated chemical compounds. ^a

Entry	Substrates	Products	t (h)	Conv. (%)	Selec. (%)
1			6	98.5	100
2			2.5	99.2	100
3			6	100	90.3
4			6	100	97.2
5			10	98	96
6			6	98.3	99
7			6	95.4	99
8			6	100	95.6
9			6	90.8	99

^a Reaction conditions: 0.5 mmol substrates in 10 ml water, 250 mg FA, Co@NG-6 catalyst (4.6 mol% Co), 160 °C.

3.7 Heterogeneity and recyclability of Co@NG-6

To prove Co@NG-6 was heterogeneous, we separated the catalyst from reaction solution after 2 h at 160 °C. Afterwards, the THD reaction was stirred for another 4 h without Co@NG-6. The vanillin conversion still remains constant (**Figure 7a**), suggesting the heterogeneous character of Co@NG-6. Furthermore, the recycling experiment of Co@NG-6 for THD of vanillin was studied in aqueous medium at 160 °C for 6 h. After reaction, the Co@NG-6 was easily separated by a strong magnet (**Figure 7b**). As shown in **Figure 7c**, conversion of vanillin was only slightly decreased from 98.5% to 91% in seven reaction runs. The selectivity of MPC remained unchanged in all cycles. After catalytic reactions, diffraction peaks of the Co phase and characteristic peaks of carbon materials were almost identical to the fresh one, as confirmed by XRD and Raman spectra (**Figure 7d, e**). Co 2p, N 1s, C 1s XPS results of recycled Co@NG-6 (**Figure 7f, S9**) were nearly identical to the fresh Co@NG-6 catalyst, which indicated that the chemical state of Co, N, C species didn't change remarkably. However, the Co content reduced slightly after seven cycles (**Table S3**), suggesting the leaching of little Co sites during seven consecutive recycling process contributed to slightly decrease of catalytic reactivity.

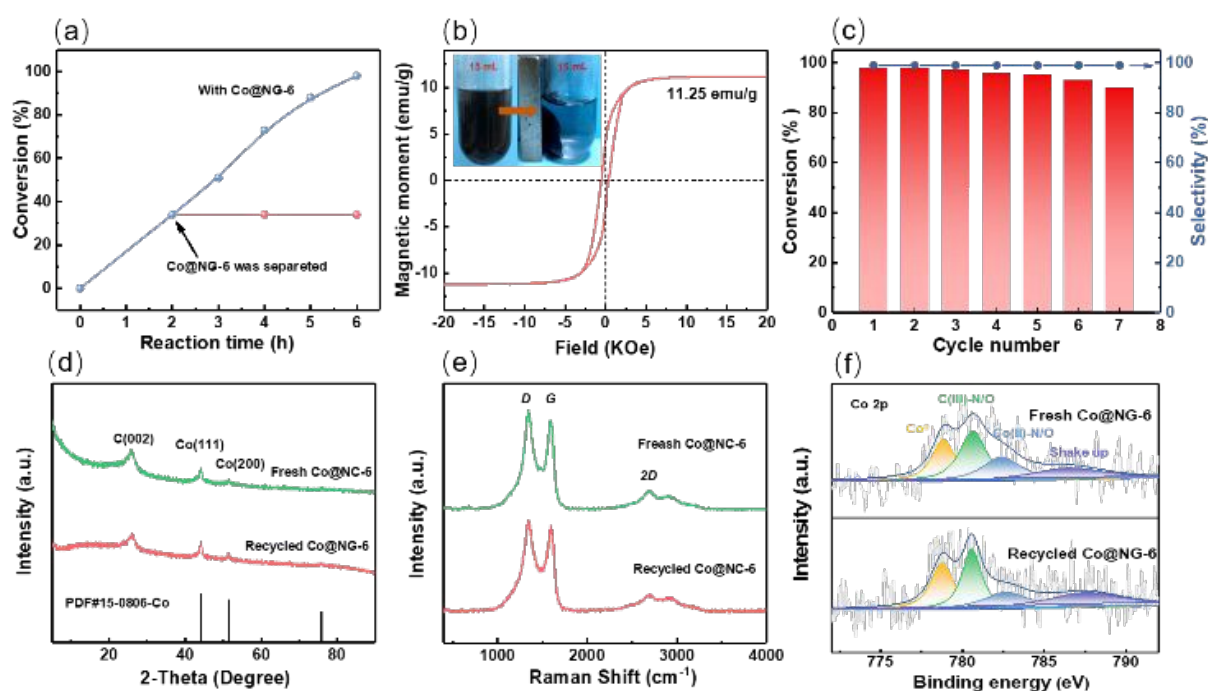


Figure 7. Heterogeneity (a) of Co@NG-6; Magnetization curve (b) of Co@NG-6 and the inset shows the magnetic separation of Co@NG-6 by using a magnet; Reusability (c) of Co@NG-6; XRD patterns (d), Raman spectra (e), Co 2p spectrum (f) of Co@NG-6 before and after reaction.

3.8 Mechanism study

There are few reports on the mechanism study of THD of biomass molecules with FA. In general, basic compounds were needed as to assist the transfer hydrogenation with FA.⁵⁴ However, we didn't add any base in THD of vanillin. In our previous experiments (**Table 1, entry 4-6 and 10**), we demonstrated that the doped-N in catalysts were of vital importance for high catalytic performance. We speculated that the N atoms in Co@NG-6 should serve as a Lewis base. To prove this, 250 mg H₃PO₄ as base poisoning reagent were added into the reaction mixture. The conversion of vanillin decreased significantly (**Table 3, Entry 1**). The strong acidic H₃PO₄ could react with basic N atoms to form NH⁺, thus poisoned the Co@NG-6. In contrast, the addition of triethylamine as additional basic sites remarkably improved the catalytic performance of Co@NG-6 (**Table 3, Entry 2**). We speculated that the cooperative role between the basic nitrogen-doped carbon/graphene and cobalt NPs via electron transfer at metal-N-graphene interface could beneficially modulates the conversion rate of THD. In fact, it was also reported in recent years that metal@C-N catalysts can serve as a Mott-Schottky type nanocatalyst with electron-deficient metal and electron-rich basic nitrogen-doped carbon/graphene.⁵⁵⁻⁵⁶ The doping of N atoms into carbon skeleton can adjust the position of valence band or conducting band of carbon phase. The flat band potential of N-doped carbon was higher than that of metal. As a result, N-enriched carbon can accept electrons from metal until their Fermi level were balanced. The electron at interface of metal and N-doped carbon can be redistributed, consequently resulting in enriched positive charges on metal. The interface Mott-Schottky effect in metal-nitrogen-carbon heterojunction can promote electron transfer to an electron-rich surface and, thus, leading to an enhanced Lewis basicity of the carbon supports (**Scheme 2a**).⁵⁷⁻⁵⁸

In our experiment, the presence of Lewis basic sites was well verified by the CO₂-TPD analysis (**Figure 4f**). Furthermore, electron paramagnetic resonance spectra (EPR) spectra (**Figure 8**) demonstrated that there was a strong interaction between the nitrogen-doped carbon/graphene and metallic Co, which was favorable for high catalytic performance by enhancing the electron transfer between metallic catalytic center and

basic N-doped support. These results further confirmed the cooperative role of Lewis basic N and encapsulated Co NPs at Mott–Schottky interface in the THD reaction. Combined with the above analysis and catalyst characterization, we proposed a feasible reaction mechanism (**Scheme 2b**).

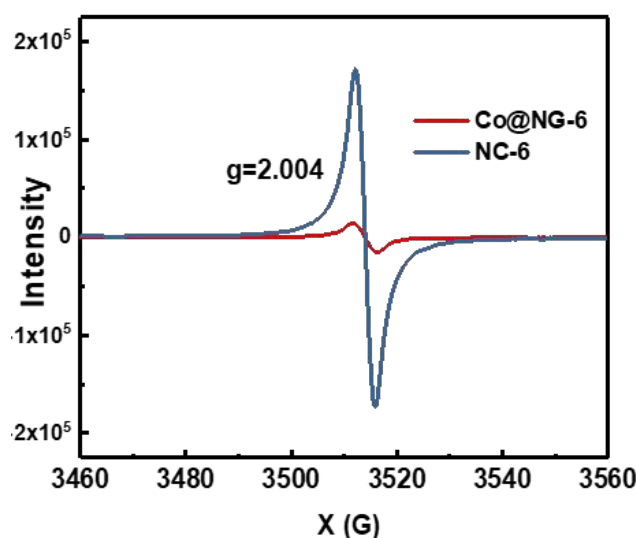


Figure 8. EPR spectra of NC-6 and Co@NG-6.

Firstly, electronegative N atoms served as Lewis basic sites in Co@NG-6 captured the H^+ from FA to form NH^+ . Simultaneously, electron negative formate intermediates can coordinate with electron-deficient Co NPs via Co^0 empty d orbitals. As a result, Co-formate intermediates were generated. In recent years, some research workers also considered that metal-formate were intermediates in the dehydrogenation reaction of FA into H_2 , when the catalysts were doped with nitrogen or basic compounds was used.⁵⁹⁻⁶¹ Afterwards, Co-hydride species ($Co-H^-$) were generated after releasing of CO_2 . The formation of NH^+ and $Co-H^-$ resembled the heterolytic cleavage of molecular hydrogen, in which doped-N or added basic compounds could promote the heterolytic cleavage. For instance, Zhang and co-workers found the doped N in Pd/N-C acted as base could enhance the heterolytic cleavage of molecular hydrogen to form protic $N-H^+$ and hydridic Pd- H^- species.⁶² Therefore, the formation of NH^+ and $Co-H^-$ was reasonable based on previous discuss and designed experimental results and these intermediates were catalytic active sites for THD of $C=O$ bonds in vanillin. Recently, protic H^+ and hydridic H^- were also generally proposed as active species for hydrogenation of polar $C=O$ or $C=N$ bonds with H_2 .^{18, 63-64} Besides, the deuterium kinetic isotope effect (KIE) experiments (**Table 3, Entry 3-6**) revealed that a large KIE of 2.79 and 3.41 was observed using DCOOH and DCOOD for THD. But the KIE was

only 1.08 when HCOOD was used as H donor. This result corroborated that the generation of Co-H⁻ via β -hydride elimination and protonation was the rate-limiting step for THD.^{18, 60}

Table 3 Effect of additives or D-substituted FA on THD of vanillin with over the Co@NG-6 catalyst.^a

Entry	Formic acid	Conv. (%)	Reaction rate	
			($\mu\text{mol min}^{-1} \text{ g catalyst}^{-1}$)	KIE ^d
1 ^b	HCOOH	18.05	5.01	-
2 ^c	HCOOH	87.05	24.18	-
3	HCOOH	51.04	14.18	-
4	HCOOD	47.24	13.12	1.08
5	DCOOH	18.33	5.09	2.79
6	DCOOD	14.99	4.16	3.41

^a Reaction conditions: 0.5 mmol vanillin in 10 mL water, 250 mg FA, Co@NG-6 catalyst (4.6 mol% metal), 160 °C, 3 h.

^b Basic sites of Co@NG-6 were poisoned by adding 300 mg phosphoric acid.

^c 120 mg triethylamine was added as additional basic sites.

^d KIE = rate (entry 3) / rate (entry n); n = 4–6.

Moreover, vanillyl alcohol is firstly generated and then hydrogenated to MPC when H₂ was used as H source. However, vanillyl alcohol cannot be detected in all reactions and MPC was the sole products (**Figure 6**). This result suggested a different reduction mechanism in comparison to other report using H₂ as H source.⁴⁶ Indeed, H₂ can form in our catalytic system via decomposition of FA because formic acid is excessive. It is reported that the generation of H₂ from active H requires more energy to overcome the overpotential of the chemisorbed H at the metal surface.⁶⁵⁻⁶⁶ In contrary, the transfer of active H to reduce vanillin over Co@NG-6 is much faster and easier than to form H₂ gas. Therefore, the formation and activation of H₂ gas was not essential for the THD of vanillin although we can detect a small amount of hydrogen from tail gas in the reactor. As a result, the reduction of vanillin proceeded by consuming four active hydrogen bonded on the surface of the Co NPs in one step. Notably, the steric hindrance caused by the encapsulation of ultrafine Co NPs in N-enriched graphene shells and strong interactions of substrate and intermediate product (vanillyl alcohol) could result in the blocking of reaction pathway toward vanillyl alcohol by steric constraints (**Scheme 2a**).⁶⁷ Besides, we found that the conversion of vanillyl alcohol was much faster than that of vanillin (**Table 2, Entry 2**). Although vanillyl alcohol can be formed in the

efficient catalysts toward base-free THD of lignin model compound vanillin with biomass-derived FA. The ionic gelation and chelation of CMC, urea and Co^{2+} contribute to uniformly dispersed Co NPs anchored on high surface area carbon skeleton, enabling the full exposure of catalytic active sites. The protected graphene-sheathed Co NPs improved the stability. Mechanism studies demonstrated that the synergistic effect between Co NPs and incorporated N via can promote the generation of Co-formate intermediates, giving impetus to form active protic H^+ and hydridic H^- for hydrogenating $\text{C}=\text{O}$ bonds. Given that all the reaction substrate, hydrogen source and catalysts in this reaction system are based on renewable biomass, we believe that our findings can pave a sustainable and promising avenue for both developing stable chainmail catalysts and efficiently upgrading of biofuel.

Acknowledgements

The authors thank the financial support for this work by the National Natural Science Foundation of China (21774036), Guangdong Province Science Foundation (2017B090903003, 2017GC010429).

Reference

- [1] J. S. Luterbacher, J. M. Rand, D. M. Alonso, J. Han, J. T. Youngquist, C. T. Maravelias, B. F. Pfleger, J. A. Dumesic, Nonenzymatic sugar production from biomass using biomass-derived γ -valerolactone, *Science*, 2014, 343, 277-280.
- [2] A. J. Ragauskas, G. T. Beckham, M. J. Biddy, R. Chandra, F. Chen, M. F. Davis, B. H. Davison, R. A. Dixon, P. Gilna, M. Keller, Lignin valorization: improving lignin processing in the biorefinery, *Science*, 2014, 344, 1246843.
- [3] R. Nie, H. Yang, H. Zhang, X. Yu, X. Lu, D. Zhou, Q. Xia, Mild-temperature hydrodeoxygenation of vanillin over porous nitrogen-doped carbon black supported nickel nanoparticles, *Green Chem.*, 2019, 21, 314-320
- [4] S. Song, J. Zhang, G. Gözaydın, N. Yan, Production of Terephthalic Acid from Corn Stover Lignin, *Angew. Chem., Int. Ed.*, 2019, 58, 4988-4991.
- [5] S. Y. Lee, H. U. Kim, T. U. Chae, J. S. Cho, J. W. Kim, J. H. Shin, D. I. Kim, Y. S. Ko, W. D. Jang, Y. S. Jang, A comprehensive metabolic map for production of bio-based chemicals, *Nat. Catal.*, 2019, 2, 18-33.
- [6] R. Fan, C. Chen, M. Han, W. Gong, H. Zhang, Y. Zhang, H. Zhao, G. Wang, Highly Dispersed Copper Nanoparticles Supported on Activated Carbon as an Efficient Catalyst for Selective Reduction of Vanillin, *Small*, 2018, 14, 1801953.
- [7] G.H. Wang, J. Hilgert, F. H. Richter, F. Wang, H.J. Bongard, B. Spliethoff, C.

- Weidenthaler, F. Schüth, Nat. Mater. Platinum–cobalt bimetallic nanoparticles in hollow carbon nanospheres for hydrogenolysis of 5-hydroxymethylfurfural, Nat. Mater., 2014, 13, 293-300. View Article Online
DOI: 10.1039/C9GC01720H
- [8] Y. T. Cheng, J. Jae, J. Shi, W. Fan, G. W. Huber, Production of renewable aromatic compounds by catalytic fast pyrolysis of lignocellulosic biomass with bifunctional Ga/ZSM-5 catalysts, Angew. Chem., Int. Ed., 2012, 51, 1387-1390.
- [9] L. Chen, C. Fink, Z. Fei, P. J. Dyson, G. Laurenczy, An efficient Pt nanoparticle–ionic liquid system for the hydrodeoxygenation of bio-derived phenols under mild conditions, Green Chem., 2017, 19, 5435-5441.
- [10] G. H. Wang, Z. Cao, D. Gu, N. Pfänder, A. C. Swertz, B. Spliethoff, H. J. Bongard, C. Weidenthaler, W. Schmidt, R. Rinaldi, Nitrogen-Doped Ordered Mesoporous Carbon Supported Bimetallic PtCo Nanoparticles for Upgrading of Biophenolics, Angew. Chem., Int. Ed., 2016, 55, 8850-8855.
- [11] K. A. Goulas, A. V. Mironenko, G. R. Jenness, T. Mazal, D. G. Vlachos, Fundamentals of C–O bond activation on metal oxide catalysts, Nat. Catal., 2019, 2, 269-276.
- [12] J. Zhang, L. D. Ellis, B. Wang, M. J. Dzara, C. Sievers, S. Pylypenko, E. Nikolla, J. W. Medlin, Control of interfacial acid–metal catalysis with organic monolayers, Nat. Catal., 2018, 1, 148-155.
- [13] D. Wang, D. Astruc, The golden age of transfer hydrogenation, Chem. Rev., 2015, 115, 6621-6686.
- [14] S. Zhou, F. Dai, Y. Chen, C. Dang, H. Qi, Sustainable hydrothermal self-assembly of hafnium–lignosulfonate nanohybrids for highly efficient reductive upgrading of 5-hydroxymethylfurfural, Green Chem., 2019, 21, 1421-1431.
- [15] G. H. Wang, X. Deng, D. Gu, K. Chen, H. Tüysüz, B. Spliethoff, H. J. Bongard, C. Weidenthaler, W. Schmidt, F. Schüth, Co₃O₄ Nanoparticles Supported on Mesoporous Carbon for Selective Transfer Hydrogenation of α,β -Unsaturated Aldehydes, Angew. Chem., Int. Ed., 2016, 55, 11101-11105.
- [16] S. Zhou, F. Dai, Z. Xiang, T. Song, D. Liu, F. Lu, H. Qi, Zirconium–lignosulfonate polyphenolic polymer for highly efficient hydrogen transfer of biomass-derived oxygenates under mild conditions, Appl. Catal. B: Environ., 2019, 248, 31-43.
- [17] D. Mellmann, P. Sponholz, H. Junge, M. Beller, Formic acid as a hydrogen storage material–development of homogeneous catalysts for selective hydrogen release, Chem. Soc. Rev., 2016, 45, 3954-3988.

- [18] P. Zhou, Z. Zhang, L. Jiang, C. Yu, K. Lv, J. Sun, S. Wang, A versatile cobalt catalyst for the reductive amination of carbonyl compounds with nitro compounds by transfer hydrogenation, *Appl. Catal. B: Environ.*, 2017, 210, 522-532.
- [19] H. H. Khoo, W. L. Ee, V. Isoni, Bio-chemicals from lignocellulose feedstock: sustainability, LCA and the green conundrum, *Green Chem.* 2016, 18, 1912-1922.
- [20] L. Xiang, S. Li, Y. Liu, C. Yong, Formic acid: A versatile renewable reagent for green and sustainable chemical synthesis, *Chin. J. Catal.* 2015, 36, 1461-1475.
- [21] K. Mori, T. Sano, H. Kobayashi, H. Yamashita, Surface Engineering of a Supported PdAg Catalyst for Hydrogenation of CO₂ to Formic Acid: Elucidating the Active Pd Atoms in Alloy Nanoparticles, *J. Am. Chem. Soc.*, 2018, 140, 8902-8909.
- [22] L. Liu, J. Li, Y. Ai, Y. Liu, J. Xiong, H. Wang, Y. Qiao, W. Liu, S. Tan, S. Feng, A ppm level Rh-based composite as an ecofriendly catalyst for transfer hydrogenation of nitriles: triple guarantee of selectivity for primary amines, *Green Chem.* 2019, 21, 1390-1395.
- [23] G. Wienhöfer, I. Sorribes, A. Boddien, F. Westerhaus, K. Junge, H. Junge, R. Llusar, M. Beller, General and selective iron-catalyzed transfer hydrogenation of nitroarenes without base, *J. Am. Chem. Soc.*, 2011, 133, 12875-12879.
- [24] I. Sorribes, G. Wienhöfer, C. Vicent, K. Junge, R. Llusar, M. Beller, Chemoselective Transfer Hydrogenation to Nitroarenes Mediated by Cubane-Type Mo₃S₄ Cluster Catalysts, *Angew. Chem., Int. Ed.*, 2012, 51, 7794-7798.
- [25] G. Li, H. Yang, H. Zhang, Z. Qi, M. Chen, W. Hu, L. Tian, R. Nie, W. Huang, Encapsulation of Nonprecious Metal into Ordered Mesoporous N-Doped Carbon for Efficient Quinoline Transfer Hydrogenation with Formic Acid, *ACS Catal.*, 2018, 8, 8396-8405.
- [26] J. Deng, P. Ren, D. Deng, X. Bao, Enhanced electron penetration through an ultrathin graphene layer for highly efficient catalysis of the hydrogen evolution reaction, *Angew. Chem. Int. Ed.*, 2015, 54, 2100-2104.
- [27] J. Shi, M. Zhao, Y. Wang, J. Fu, X. Lu, Z. Hou, Upgrading of aromatic compounds in bio-oil over ultrathin graphene encapsulated Ru nanoparticles, *J. Mater. Chem. A*, 2016, 4, 5842-5848.
- [28] A. Kasprzak, M. Bystrzejewski, M. Koszytkowska-Stawinska, M. Poplawska, Grinding-induced functionalization of carbon-encapsulated iron nanoparticles, *Green Chem.*, 2017, 19, 3510-3514.
- [29] X. Cui, P. Ren, D. Deng, J. Deng, X. Bao, Single layer graphene encapsulating

non-precious metals as high-performance electrocatalysts for water oxidation, *Energy Environ. Sci.*, 2016, 9, 123-129. View Article Online
DOI: 10.1039/C5GC01720H

[30] Y. Xu, W. Tu, B. Zhang, S. Yin, Y. Huang, M. Kraft, R. Xu, Nickel Nanoparticles Encapsulated in Few-Layer Nitrogen-Doped Graphene Derived from Metal-Organic Frameworks as Efficient Bifunctional Electrocatalysts for Overall Water Splitting, *Adv. Mater.*, 2017, 29, 1605957.

[31] D. Das, A. Das, M. Reghunath, K. Kar Nanda, Phosphine-free avenue to Co₂P nanoparticle encapsulated N,P co-doped CNTs: a novel non-enzymatic glucose sensor and an efficient electrocatalyst for oxygen evolution reaction, *Green Chem.*, 2017, 19, 1327-1335

[32] F. Bu, P. Xiao, J. Chen, M. F. Aly Aboud, I. Shakir, Y. Xu, Rational design of three-dimensional graphene encapsulated core-shell FeS@carbon nanocomposite as a flexible high-performance anode for sodium-ion batteries, *J. Mater. Chem. A*, 2018, 6, 6414-6421.

[33] J. Deng, D. Deng, X. Bao, Robust catalysis on 2D materials encapsulating metals: concept, application, and perspective, *Adv. Mater.*, 2017, 29, 1606967.

[34] Y. Li, T. Gao, Y. Yao, Z. Liu, Y. Kuang, C. Chen, J. Song, S. Xu, E. M. Hitz, B. Liu, R.J. Jacob, M.R. Zachariah, G. Wang, L. Hu, In Situ "Chainmail Catalyst" Assembly in Low-Tortuosity, Hierarchical Carbon Frameworks for Efficient and Stable Hydrogen Generation, *Adv. Energy Mater.*, 2018, 8, 1801289.

[35] Z. Wei, J. Wang, S. Mao, D. Su, H. Jin, Y. Wang, F. Xu, H. Li, H. Y. Wang, In Situ-Generated Co₀-Co₃O₄/N-Doped Carbon Nanotubes Hybrids as Efficient and Chemoselective Catalysts for Hydrogenation of Nitroarenes, *ACS Catal.*, 2015, 5, 4783-4789.

[36] H. Yang, R. Nie, W. Xia, X. Yu, D. Jin, X. Lu, D. Zhou, Q. Xia, Co embedded within biomass-derived mesoporous N-doped carbon as an acid-resistant and chemoselective catalyst for transfer hydrodeoxygenation of biomass with formic acid, *Green Chem.*, 2017, 19, 5714-5722.

[37] L. Liu, S. Ci, L. Bi, J. Jia, Z. Wen, Three-dimensional nanoarchitectures of Co nanoparticles inlaid on N-doped macroporous carbon as bifunctional electrocatalysts for glucose fuel cells, *J. Mater. Chem. A*, 2017, 5, 14763-14774.

[38] H. Xu, S. Ci, Y. Ding, G. Wang, Z. Wen, Recent advances in precious metal-free bifunctional catalysts for electrochemical conversion systems, *J. Mater. Chem. A*, 2019, 7, 8006-8029.

[39] S. Li, G. Zhang, X. Tu, J. Li, Polycrystalline CoP/CoP₂ structures for efficient full water splitting, *ChemElectroChem*, 2018, 5, 701-707.

- [40] P. Ren, S. Ci, Y. Ding, Z. Wen, Molten-salt-mediated synthesis of porous Fe₃C containing N-doped carbon as efficient cathode catalysts for microbial fuel cells, *Appl. Surf. Sci.*, 2019, 481, 1206-1212. View Article Online
DOI: 10.1059/C9GC01720H
- [41] A. Szabolcs, M. Molnár, G. Dibó, T.M. László, Microwave-assisted conversion of carbohydrates to levulinic acid: An essential step in biomass conversion, *Green Chem.*, 2017, 15, 439-445.
- [42] P. Bhaumik, P. L. Dhepe, Conversion of biomass into sugars. Biomass sugars for non-fuel applications. Royal Society Chemistry, 2015, Chapter 1, 1-53.
- [43] H. Qi, B. Schulz, T. Vad, J. Liu, E. Mäder, G. Seide, T. Gries, Novel carbon nanotube/cellulose composite fibers as multifunctional materials, *ACS Appl. Mater. Interfaces.*, 2015, 7, 22404–22412.
- [44] Y. Chen, P. Pötschke, J. Pionteck, B. Voit, H. Qi, Smart cellulose/graphene composites fabricated by in situ chemical reduction of graphene oxide for multiple sensing applications, *J. Mater. Chem. A*, 2018, 6, 7777-7785.
- [45] S. Zhou, G. Chen, F. Xiao, W. Ming, H. Qi, In situ MnO_x/N-doped carbon aerogels from cellulose as monolithic and highly efficient catalysts for the upgrading of bioderived aldehydes, *Green Chem.* 2018, 20, 3593.
- [46] C. B. Godiya, X. Cheng, D. Li, Z. Chen, X. Lu, Carboxymethyl cellulose/polyacrylamide composite hydrogel for cascaded treatment/reuse of heavy metal ions in wastewater, *J. Hazard. Mater.* 2019, 364, 28-38.
- [47] W. Yang, X. Liu, X. Yue, J. Jia, S. Guo, Bamboo-like Carbon Nanotube/Fe₃C Nanoparticle Hybrids and Their Highly Efficient Catalysis for Oxygen Reduction, *J. Am. Chem. Soc.* 2015, 137, 1436-1439.
- [48] Q. Bi, J. Lin, Y. Liu, H. He, F. Huang, Y. Cao, Dehydrogenation of Formic Acid at Room Temperature: Boosting Palladium Nanoparticle Efficiency by Coupling with Pyridinic-Nitrogen-Doped Carbon, *Angew. Chem., Int. Ed.*, 2016, 55, 11849-11853.
- [49] H. Su, P. Gao, M. Y. Wang, G. Y. Zhai, J. J. Zhang, T. J. Zhao, J. Su, M. Antonietti, X. H. Li, J. S. Chen, Grouping Effect of Single Nickel–N₄ Sites in Nitrogen-Doped Carbon Boosts Hydrogen Transfer Coupling of Alcohols and Amines, *Angew. Chem., Int. Ed.*, 2018, 57, 15194-15198.
- [50] S. Tian, Z. Wang, W. Gong, W. Chen, Q. Feng, Q. Xu, C. Chen, C. Chen, Q. Peng, L. Gu, H. Zhao, P. Hu, D. Wang, Y. Li, Temperature-Controlled Selectivity of Hydrogenation and Hydrodeoxygenation in the Conversion of Biomass Molecule by the Ru₁/mpg-C₃N₄ Catalyst, *J. Am. Chem. Soc.*, 2018, 140, 11161-11164.
- [51] W. Feng, H. Dong, L. Niu, X. Wen, L. Huo, G. Bai, A novel Fe₃O₄@nSiO₂@

- NiPd–PVP@mSiO₂ multi-shell core–shell nanocomposite for cinnamic acid hydrogenation in water, *J. Mater. Chem. A*, 2015, 3, 19807-19814.
- [52] N. S. Date, A. M. Hengne, K. W. Huang, R. C. Chikate, C. V. Rode, Single pot selective hydrogenation of furfural to 2-methylfuran over carbon supported iridium catalysts, *Green Chem.*, 2018, 20, 2027-2037.
- [53] L. Lin, S. Yao, R. Gao, X. Liang, Q. Yu, Y. Deng, J. Liu, M. Peng, Z. Jiang, S. Li, Y. Li, X. Wen, W. Zhou, D. Ma, A highly CO-tolerant atomically dispersed Pt catalyst for chemoselective hydrogenation, *Nat. Nanotechnol.*, 2019, 1, 354-361.
- [54] R. V. Jagadeesh, K. Natte, H. Junge, M. Beller, Nitrogen-doped graphene-activated iron-oxide-based nanocatalysts for selective transfer hydrogenation of nitroarenes, *ACS Catal.*, 2015, 5, 1526-1529.
- [55] Y. Liu, H. Wang, T. Zhao, B. Zhang, H. Su, Z. Xue, X. Li, J. Chen, Schottky Barrier Induced Coupled Interface of Electron-Rich N-Doped Carbon and Electron-Deficient Cu: In-Built Lewis Acid–Base Pairs for Highly Efficient CO₂ Fixation, *J. Am. Chem. Soc.*, 2018, 141, 38-41.
- [56] H. Zhou, H. Xu, Y. Liu, Aerobic oxidation of 5-hydroxymethylfurfural to 2, 5-furandicarboxylic acid over Co/Mn-lignin coordination complexes-derived catalysts, *Appl. Catal. B: Environ.* 2019, 244, 965-973.
- [57] H. Su, K. Zhang, B. Zhang, H. Wang, Q. Yu, X. Li, M. Antonietti, J. Chen, Activating cobalt nanoparticles via the Mott–Schottky effect in nitrogen-rich carbon shells for base-free aerobic oxidation of alcohols to esters, *J. Am. Chem. Soc.*, 2017, 139, 811-818.
- [58] Y. Cai, X. Li, Y. Zhang, X. Wei, K. Wang, J. Chen, Highly Efficient Dehydrogenation of Formic Acid over a Palladium-Nanoparticle-Based Mott–Schottky Photocatalyst, *Angew. Chem., Int. Ed.*, 2013, 52, 11822-11825.
- [59] B. Albert, M. Dörthe, G. R. Felix, J. Ralf, J. Henrik, P. J. Dyson, L. Gábor, L. Ralf, B. Matthias, Efficient dehydrogenation of formic acid using an iron catalyst, *Science*, 2011, 333, 1733-1736.
- [60] Q. Bi, X. Du, Y. Liu, Y. Cao, H. He, K. Fan, Efficient subnanometric gold-catalyzed hydrogen generation via formic acid decomposition under ambient conditions, *J. Am. Chem. Soc.*, 2012, 134, 8926-8933.
- [61] Q. Liu, X. Yang, Y. Huang, S. Xu, X. Su, X. Pan, J. Xu, A. Wang, C. Liang, X. Wang, A Schiff base modified gold catalyst for green and efficient H₂ production from formic acid. *Energy Environ. Sci*, 2015, 8, 3204-3207.

- [62] S. Wang, P. Zhou, L. Jiang, Z. Zhang, K. Deng, Y. Zhang, Y. Zhao, J. Li, S. Bottle, H. Zhu, Selective deoxygenation of carbonyl groups at room temperature and atmospheric hydrogen pressure over nitrogen-doped carbon supported Pd catalyst, *J. Catal.*, 2018, 368, 207-216. View Article Online
DOI: 10.1039/C9GC01720H
- [63] E. B. Hulley, K. D. Welch, A. M. Appel, D. L. DuBois, R. M. Bullock, Reversible Heterolytic Cleavage of Bound H₂, *J. Am. Chem. Soc.*, 2013, 135, 11736-11739.
- [64] T. Liu, X. Wang, C. Hoffmann, D. L. DuBois, R. M. Bullock, Heterolytic Cleavage of Hydrogen by an Iron Hydrogenase Model: An Fe-H... H-N Dihydrogen Bond Characterized by Neutron Diffraction, *Angew. Chem., Int. Ed.*, 2014, 53, 5300-5304.
- [65] M. Elam, B. E. Conway, State of overpotential-deposited H species at electroplated platinum surfaces in comparison with bright platinum, *J. Appl. Electrochem.*, 1987, 17, 1002-1020.
- [66] L. Gong, Y. Cai, X. Li, Y. Zhang, J. Su, J. Chen, Room-temperature transfer hydrogenation and fast separation of unsaturated compounds over heterogeneous catalysts in an aqueous solution of formic acid, *Green Chem.*, 2014, 16, 3746-3751.
- [67] A. Aijaz, Q. Zhu, N. Tsumori, Q. Xu, Surfactant-free Pd nanoparticles immobilized to a metal-organic framework with size-and location-dependent catalytic selectivity, *Chem. Commun.*, 2015, 51, 2577-2580.